Astron. Astrophys. 334, 57–70 (1998)

ASTRONOMY
AND
ASTROPHYSICS

Radio-FIR correlations within M 31⋆

P. Hoernes[1], **E.M. Berkhuijsen**[1], **and C. Xu**[2⋆⋆]

[1] Max-Planck-Institut für Radioastronomie, Auf dem Hügel 69, D-53121 Bonn, Germany
[2] Max-Planck-Institut für Kernphysik, Saupfercheckweg 1, D-69117 Heidelberg, Germany

Received 12 January 1998 / Accepted 18 February 1998

Abstract. We present a study of the relationship between the surface brightness of the radio continuum emission and the FIR emission within M 31, based on radio maps at four wavelengths (73 cm, 20 cm, 11 cm and 6 cm) and the HIRES-FIR maps at $60\,\mu$m and $100\,\mu$m. For a common resolution of $5'$ we decomposed the radio emission into a thermal and a nonthermal radio continuum map at λ20 cm, and the FIR emission into emission from warm (27 K) and cool (19 K) dust. The good angular resolutions of the maps ($5'$, $3'$ and $2'$) allowed the use of rigorous statistical methods to determine the slopes of the correlations. We obtained the following results:

1. In the region $30' < R < 90'$, at all three resolutions corresponding to 1×5 kpc down to 0.4×2 kpc in the plane of M 31, the total radio emission is significantly correlated with the total FIR emission, even after correction for the general radial decrease. In the latter case, the slope of the λ20 cm-radio/total-FIR relation is unity. Also in the inner disk ($R < 30'$) of M 31 the total radio emission at λ20 cm correlates significantly with total FIR emission after radial correction; the slope is also unity in spite of the fact that in the inner disk the dust temperatures are quite different from those in the outer disk.

2. After radial correction significant correlations exist in the outer disk on a scale of a few kpc between thermal radio and warm dust emission as well as between nonthermal radio and cool dust emission, with slopes of 1.17 ± 0.13 and 0.80 ± 0.09, respectively.

The thermal-radio/warm-dust correlation is expected from the common dependence of the two emissions on the massive ionizing stars. However, the nonthermal-radio/cool-dust correlation cannot be explained by a common dependence on the energy sources, because the heating of the cool dust is dominated by the ISRF. Instead, we propose that this correlation arises because of a coupling of the magnetic field to the gas which is mixed with the cool dust. This 'magnetic field-gas coupling' model can explain the slope ≤ 1 of the nonthermal-radio/cool-dust correlation if energy equipartition between cosmic-ray electrons and magnetic fields is not valid on scales ≤ 2 kpc.

Key words: galaxies: individual: M 31 – galaxies: ISM – radio continuum: galaxies – infrared: galaxies

1. Introduction

One of the most important discoveries of the IRAS mission was the correlation between the far infrared (FIR) and the radio continuum luminosities of galaxies (de Jong et al. 1985; Helou et al. 1985). The most outstanding features of this correlation are (1) the extreme tightness (spanning 5 orders of magnitude with a dispersion of only 50%) and (2) the universality (followed by all galaxies with ongoing star formation without AGN (Wunderlich et al. 1987; Niklas 1997)). Xu et al. (1994a) showed that the correlation cannot be explained by a mass-scaling (richness) effect, but depends on intrinsic properties, such as the star-formation rate per unit mass, influencing different processes in a galaxy.

It is widely accepted that the basic reason for the *existence* of the FIR-radio correlation is the dependence of both emissions on the recent star-formation activity present in galaxies of all types (see Condon 1992, and Völk & Xu 1994, for reviews). Massive stars ($> 20\,\mathrm{M}_\odot$) ionize the gas and heat the dust, giving rise to thermal radio emission and thermal emission from warm dust, whereas intermediate-mass stars (5-$20\,\mathrm{M}_\odot$) largely power the cool dust (Xu 1990). All these stars are progenitors of supernovae and supernova remnants, which are the sources of the relativistic electrons that radiate the synchrotron emission. At cm and dm wavelengths the radio emission is mainly nonthermal (Gioia et al. 1982; Niklas 1997). A significant part of the FIR emission is from cool dust ('FIR cirrus') (Buat & Deharveng 1988; Xu et al. 1994b).

Several theoretical models have been proposed to explain the slope (> 1; the radio luminosity increases slightly faster than the FIR luminosity) and the tightness of the correlation. The main difference between these models is in the assumption of optical thickness of galaxies to the radiation of stars powering the FIR emission and the relativistic electrons radiating the nonthermal radio continuum.

Send offprint requests to: E.M. Berkhuijsen

⋆ Appendices A, B and C only appear in the electronic version of this paper

⋆⋆ *Present address:* IPAC, M/S 100-22, California Institute of Technology, Pasadena CA 91125, USA

Models based on the assumptions that galaxies are 'optically thick' to relativistic electrons and UV photons were proposed by Völk (1989), Völk & Xu (1994), and Lisenfeld et al. (1996). In these 'calorimeter models' the relativistic electrons mainly responsible for the observed nonthermal emission lose most of their energy in the galaxy before they escape. Likewise, most of the relevant UV energy is converted into the FIR. Since the production rates of both the relativistic electrons and the UV photons are proportional to massive and intermediate-mass stars, these models give a straightforward explanation for the tightness of the correlation. The slight non-linearity of the correlation ($P_{\rm rad} \propto L_{\rm fir}^{(1.3)}$) can be largely attributed to the contribution of radio-quiet, old stars to the FIR emission (Condon et al. 1991; Xu et al. 1994a), although the weak dependence of the radio power on the magnetic field may also play a role (Lisenfeld et al. 1996).

On the other hand, Helou & Bicay (1993) proposed that the escape lengths of relativistic electrons and UV photons are proportional, in which case galaxies optically thin to UV photons are also 'optically thin' to relativistic electrons. In addition, they assumed a close coupling between magnetic field strength and gas density, and proportionality between relativistic electrons and dust-heating photons with young stars as their common source. Based also on an 'optically thin' model, Chi & Wolfendale (1990) interpreted the nonlinearity of the correlation in terms of the dependence of the escape rate of the relativistic electrons on the FIR luminosity. The limitation of the models optically thin in UV is that they only apply to a minority of the galaxies that follow the correlation. Buat & Xu (1996) and Lisenfeld et al. (1996) showed that most galaxies are optically thick to dust-heating UV photons.

Recently Niklas & Beck (1997) challenged the calorimeter theory by arguing that in 70% of the galaxies in their sample the CR electrons do not lose much energy before they escape, as the relatively flat synchrotron spectra (spectral index $\alpha > -0.9$) of these galaxies indicate. This could mean that most galaxies are optically thick to UV photons but 'optically thin' to CR electrons, a case not covered by either 'optically thick' or 'optically thin' models. In the empirical approach of Niklas & Beck (1997) the basic variable is the average volume density of the (total) gas, on which both the star formation, that powers the FIR, and the magnetic field strength, that determines the synchrotron emission, depend. Using the observed relationships, they found the correct slope for the radio-FIR correlation. However, it is not clear why this correlation should be so tight.

In summary, there is still no consensus on the question why the radio-FIR correlation exists and why it is so tight. This lead many authors to investigate the *local* radio-FIR correlation, that is *within* nearby galaxies (Beck & Golla 1988; Rice et al. 1988; Bicay et al. 1989; Bicay & Helou 1990; Xu et al. 1992; Fitt et al. 1992; Marshall & Helou 1995; Lu et al. 1996), which may provide detailed information on how the correlation works. The results may be summarized as follows. (1) Generally the peaks of the two emissions are in close correspondence. (2) The surface-brightness distribution of the FIR has a larger dynamic range than that of the radio continuum emission and it also has a shorter radial scale length than the radio emission; both phenomena can be explained by the diffusion of CR electrons (Boulanger & Pérault 1988; Bicay & Helou 1990; Lu et al. 1996).

However, in most of these studies either the radio emission (consisting of thermal and nonthermal emission) or the FIR emission (consisting of a warm component due to the emission of dust associated with H II regions and a cool component due to diffuse cirrus heated by the ISRF) was not decomposed. It may well be that the good correspondence between the peaks in the FIR and radio maps are purely due to the trivial correlation between the thermal radio emission and the dust emission associated with H II regions (Xu et al. 1992). Although globally nonthermal radio luminosities correlate strongly with the luminosities of the diffuse (cirrus) FIR component (Xu et al. 1994b), we do not know whether this also holds within a galaxy. Furthermore, none of the authors who studied the local radio-FIR correlation corrected for the general radial decrease of the emissions, which partially accounts for the correlation, or used a rigorous statistical method.

In this paper we make a comprehensive statistical study on the radio-FIR correlation within M 31, the Andromeda Galaxy. The emphasis is on the synchrotron/cool-dust correlation. We chose M 31 because of the following reasons:

1. As M 31 is the nearest spiral galaxy and extends more than 3 degrees along the major axis, it is well resolved both in radio and in FIR.

2. Its radio emission is dominated by the nonthermal component (Beck & Gräve 1982), and its FIR is dominated by the cool dust emission (Walterbos & Schwering 1987; Xu & Helou 1996a; but see also Devereux et al. 1994).

3. It has a very low present-day star-formation rate, which is about an order of magnitude lower than that of the Galaxy (Walterbos 1987; Xu & Helou 1996a). At the same time it lies on the regression line of the global radio-FIR correlation (Helou et al. 1985; Niklas 1997).

In Sect. 2, we compare the radio continuum maps of M 31 with the FIR maps; the decomposition of the FIR and radio maps is described in Sect. 3. Results of selected correlations between the radio and FIR components are presented in Sect. 4. Physical interpretations of the results are given in Sect. 5, they are followed by a discussion in Sect. 6 and concluding remarks in Sect. 7. In Appendix B we present the full set of correlation results.

2. FIR and radio maps

2.1. The data

The radio maps used are the new λ6 cm Effelsberg survey (Berkhuijsen et al., in prep.), the λ11 cm Effelsberg survey (Beck at al. 1980), the new VLA 20 cm survey combined with Effelsberg data at the same frequency (Beck et al. 1998) and the λ73 cm continuum survey (Gräve et al. 1980). The FIR maps were made from high-resolution IRAS maps at 60 μm and 100 μm as published by Xu & Helou (1996a). We subtracted the strong nuclear point-like feature from all radio and

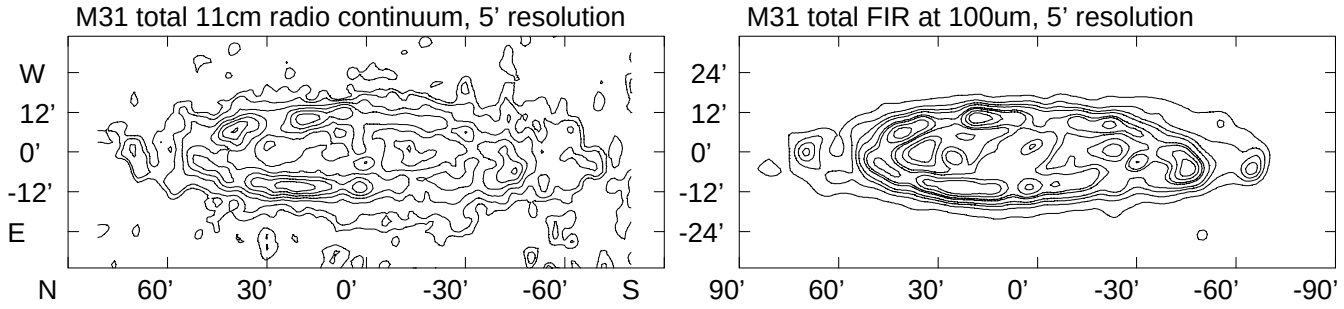

Fig. 1. The Effelsberg map at $\lambda 11$ cm of the total radio continuum emission (left) at $5'$ resolution and the map of total FIR at 100 μm (right) at the same resolution. From both maps the point-like nuclear source was subtracted. The contour lines in the maps indicate 2, 4, 6, 8, 12, 16 and 20 times the r.m.s. noise.

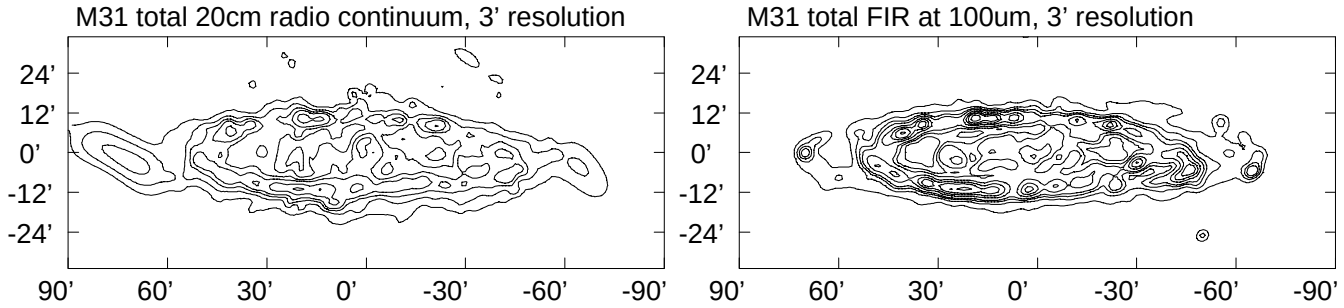

Fig. 2. The combined Effelsberg/VLA radio map of the total emission at 20 cm (left) and the map of total FIR emission (right), both at a resolution of $3'$. Outside $60'$ from the centre near the major axis no VLA pointings are available and the resolution of the $\lambda 20$ cm map degrades to the Effelsberg resolution of about $9'$. From both maps the point-like nuclear source was subtracted. The contour lines in the maps indicate 2, 4, 6, 8, 12, 16 and 20 times the r.m.s. noise.

FIR maps before processing them further in order to enable a comparison of the extended emission in the disk near the centre. See Appendix A for detailed information on the final maps. The residual emission near the centre visible on Figs. 1 to 4 is extended emission from the inner filamentary and spiral structures visible on high-resolution maps at radio and FIR wavelengths and in Hα (Beck et al. 1998; Xu & Helou 1996a, Ciardullo et al. 1988). We used $(\alpha_{50}, \delta_{50}) = (0^{\rm h}40^{\rm m}1\overset{\rm s}{.}8,\ +40°59'46'')$ as the centre position of M 31 and a position angle of the major axis of $38°$. Positive coordinates along the major and the minor axis describe regions north and west of the centre, respectively.

In Fig. 1 we present the maps of total radio continuum emission at $\lambda 11$ cm and total FIR emission, both smoothed to a resolution of $5'$; this corresponds to a linear scale of 1 kpc along the major axis and 4.8 kpc along the minor axis, assuming an inclination angle of $78°$ (Braun 1991).

The combination of the $\lambda 20$ cm VLA survey of M 31 with Effelsberg data (Beck et al. 1998) made it possible to go to higher angular resolutions. In Fig. 2 the 20 cm radio continuum map and the FIR emission are shown at a common resolution of $3'$ corresponding to 600 pc $\times$ 2.8 kpc in M 31.

2.2. Comparison of maps

The radio and FIR maps in Figs. 1 and 2 show striking similarity: all are dominated by the famous 'ring' at 8-10 kpc, and the brightest features, mostly giant star-forming regions, correlate with each other in morphology and brightness. The regions of strongest emission visible in the $5'$ maps are situated in the northeast (NE: $25', -10'$), northwest (NW: $18', 12'$ and $30', 12'$) and southwest (SW: $-24', 12'$). On the southern major axis an extended region (S: $-45', -5'$) of strong emission is situated. The same regions are prominent in the $3'$ maps. Generally we see a higher contrast between regions of high emission and other parts of the 'ring' in the FIR maps than in the radio maps.

In the 11 cm map at $5'$ resolution elongated features apparently connecting the western and eastern arms are more or less parallel to the minor axis but run from NE to SW in the FIR maps. These are actually inner arms shortened by the effect of the high inclination of $78°$; they are clearly visible on the original FIR maps at a resolution of $1'.7$ (Xu & Helou 1996). The region at (S: $-45', -5'$) shows strong extended emission both in radio and in FIR at $5'$ resolution, which consists of several sources at $3'$. In this region the largest molecular cloud complexes in M 31 are situated.

The emission seen outside the 'ring' (at $70', 0'$ and $-70', 0'$) comes from outer spiral arms of M 31 known from early optical, radio, and H I observations (Baade 1958; Berkhuijsen 1977; Emerson 1974).

The close similarities between the radio and FIR maps indicate that a local correlation between radio continuum and FIR radiation exists. In this paper we quantitatively analyze these correlations and discuss underlying physical principles. To carry out this task it is necessary to decompose our FIR and radio maps

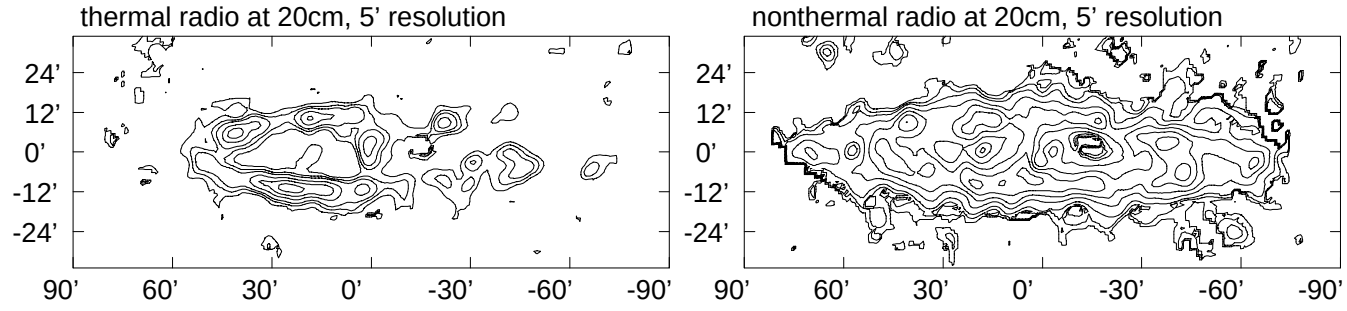

Fig. 3. Thermal and nonthermal radio continuum emission of M 31 at a resolution of $5'$ calculated for λ20 cm derived from radio maps without nuclear point sources. The contour lines in the maps indicate 2, 4, 6, 8, 12, 16 and 20 times the r.m.s. noise of the λ20 cm total radio map.

given the two-component nature of both the radio and the FIR emission.

3. Decomposition of emission

3.1. Radio decomposition

The radio continuum emission from galaxies is due to two emission mechanisms: nonthermal (synchrotron) radiation and thermal radiation from ionized regions. As the nonthermal radiation has a flux-density spectral index of typically < -0.7 and the thermal radiation of -0.1 it is possible to calculate the thermal and the nonthermal fractions from Eq. (1) if maps at at least two frequencies are available,

$$I(\nu) = I_{\rm nth} * \nu^{\alpha_n} + I_{\rm th} * \nu^{-0.1} \,, \qquad (1)$$

where $I_{\rm nth}$ and $I_{\rm th}$ are the nonthermal and thermal brightnesses (or flux densities per beam area), respectively, at frequency $\nu = 1$ and $\alpha_{\rm n}$ is the nonthermal spectral index. Beck & Gräve (1982) determined the mean nonthermal spectral index between 7 kpc and 12 kpc in M 31 to be -0.88 ± 0.05, with a tendency to steepen beyond a radius of 14 kpc (or $70'$ on the major axis). Between 1 kpc and 4 kpc from the centre $\alpha_{\rm n}$ is not known. As Beck & Gräve used the H II-region distribution of Pellet et al. (1978), the map of thermal emission obtained by using their value of $\alpha_{\rm n}$ is not entirely indedepent of the H II-region distribution. On the other hand, a value of $\alpha_{\rm n} \simeq -0.90$ is also indicated by the total spectral index near 15 kpc radius where the influence of H II regions is small.

We solved the minimization problem given by Eq. (1) by using the ODRPACK routines to perform a weighted linear least-square fit (Boggs et al. 1992). ODRPACK was applied to fit Eq. (1) to all the points where all four maps at $5'$ resolution (6 cm, 11 cm, 20 cm and 73 cm, see Sect. 2) are brighter than 2σ r.m.s. noise.

We generated a thermal radio and a nonthermal radio map at λ20 cm assuming a fixed nonthermal spectral index of -0.88 all over the map. The total flux density of the thermal emission at λ20 cm then is 0.8 ± 0.1 Jy whereas the nonthermal emission accounts for 3.3 ± 0.2 Jy[1] (the errors given do not include decomposition errors). With 19% thermal emission at λ20 cm M 31 is clearly dominated by the nonthermal component. In Fig. 3 the results of the radio continuum decomposition are shown. The morphology of the thermal emission resembles that of the Hα emission published by Devereux et al. (1994) and is dominated by the star-forming regions. The similarity between these two maps indicates that a constant value of $\alpha_{\rm n} = -0.88$ is appropriate. A value of $\alpha_{\rm n} < -0.88$ merely results in an increase of the thermal emission and a decrease of the nonthermal emission without changing the morphology significantly. The nonthermal emission has a much smoother distribution than the thermal emission, and the emission from the 'ring' is only slightly brighter than the disk emission. The decomposition agrees well with the results of Beck & Gräve (1982) based on only two frequencies.

The decomposition was also done at a resolution of $3'$ using the radio maps at λ6 cm and λ20 cm. The total flux densities of the thermal and nonthermal components at λ20 cm at $3'$ are 0.9 ± 0.1 Jy and 3.0 ± 0.2 Jy, in good agreement with the values at $5'$ resolution. However, because of the baseline problems in the λ20 cm map we could not use these decomposed maps for correlations with the FIR maps (see Appendix B).

3.2. FIR decomposition

In the $60\,\mu$m and $100\,\mu$m bands covered by IRAS two important dust components can be distinguished that contribute to the FIR emission: warm dust associated with H II regions, heated by ionizing massive ($> 20\,{\rm M}_\odot$) stars, and cool dust (cirrus) mainly heated by the ISRF which is powered by non-ionizing stars (Helou 1986; Walterbos & Schwering 1987). Unlike the two components in the radio continuum, both dust components radiate thermal emission. The warm and the cool component can be separated by assuming that the dust emission follows a λ^{-2}-law and that each component has a constant temperature, corresponding to a fixed ratio $B_{60\,\mu{\rm m}}/B_{100\,\mu{\rm m}}$. For each point in the map the intensity of each component can then be obtained from the local $B_{60\,\mu{\rm m}}/B_{100\,\mu{\rm m}}$ ratio. This decomposition method has been widely used in the literature (see Soifer et al. (1987) for a review). The method has several shortcomings. First, it is unphysical to assume a single dust temperature for

[1] This value is a lower limit as points weaker than 2σ, which are mainly nonthermal, are not included. Subtraction of the thermal component from the total flux density of 4.2 ± 0.5 Jy (Beck et al. 1998) yields 3.4 ± 0.5 Jy for the nonthermal emission.

each component. The assumed temperatures are *equivalent* temperatures and heavily weighted by the physically hottest dust in each component. At $\lambda 60\,\mu$m also very small grains with non-equilibrium heating may contribute significantly (Walterbos & Schwering 1987). Second, the result is sensitive to the assumed colour temperatures of the two components. Nevertheless, we used this method for the sake of simplicity, with the justification that the resulting warm component has the same morphology as the regions of star formation, except in the bulge (see below), as is expected on physical grounds. Bearing in mind the caveats discussed above, we tried several pairs of grain temperature for the warm and the cool component to estimate the uncertainty due to the assumption of constant grain temperatures.

In the decomposition carried out by Walterbos & Schwering (1987), the warm component was assumed to have a grain temperature of 40 K (λ^{-2}-emissivity law) and the cool component of 21 K. Xu & Helou (1996a), who separated the sources and the diffuse FIR emission using the new high-resolution IRAS maps of M 31, found that the mean temperature of H II-region associated dust is only 26 ± 1 K ($B_{60\,\mu\mathrm{m}}/B_{100\,\mu\mathrm{m}} = 0.30 \pm 0.04$), much lower than that assumed by Walterbos & Schwering. The mean colour temperature of diffuse dust in the M 31 disk, away from star formation regions, is 20 ± 1 K ($B_{60\,\mu\mathrm{m}}/B_{100\,\mu\mathrm{m}} = 0.15 \pm 0.04$) consistent with the value taken by Walterbos & Schwering. Unlike the dust associated with H II regions which shows significant fluctuations in FIR colour temperature, the diffuse dust in the M 31 disk has a rather constant $B_{60\,\mu\mathrm{m}}/B_{100\,\mu\mathrm{m}}$ ratio (Walterbos & Schwering 1987). This is widely accepted as a sign of the existence of small grains (see Puget & Léger (1989) for a review). It should be noted that near the nucleus of M 31, where there is little star formation but where the density of old stars is very high, the dust temperature is as high as ~ 30 K, higher than in any H II region in M 31 (Xu & Helou 1994). This shows that the 'cool' component is *not* always cooler than the 'warm' component.

We performed the decomposition with a warm dust temperature of 27 K as well as with 35 K, and a cool dust temperature of 19 K using the formula given by Condon et al. (1991). The choice of temperatures does not much influence the morphology of the warm and cool dust emissions but rather their relative brightness. In Fig. 4 we present the results of the decomposition with temperatures of cool and warm dust of 19 K and 27 K, respectively.

As expected the map of the warm dust emission shows resemblence with the Hα map presented by Devereux et al. (1994). The regions of strong emission from warm dust are all known as star-forming regions and are also bright in Hα.

The map of the cool dust emission shows strong arm- or ring-like structures, but the star-forming regions have almost disappeared. The arm/disk contrast is weaker than in the warm dust map. The total flux density in the warm dust map is 1070 Jy, in the cool dust map 1910 Jy. With 64% cool dust radiation the cool component is indeed dominating. The flux density of the warm component is almost equal to the flux density of the 'H II-associated' component determined by Xu & Helou (1996a). This suggests that the warm dust emission mainly originates from star-forming regions.

Xu & Helou (1994) carried out an alternative attempt to decompose the FIR radiation. They extracted point-like sources with a surface brightness of at least 1 MJy/sr above background from the 60 μm map. The application of this method resulted in 21% source emission and 79% residual diffuse emission. The emission from FIR sources is smaller than that from warm dust, because any spread-out warm dust associated with faint H II regions or diffuse Hα is not included (Xu & Helou, 1996a).

4. Radio-FIR correlations

4.1. The statistical method

We are dealing with two sets of observed variables which we have to treat symmetrically as none is directly dependent on the other. The errors in the measurements are the noise errors in the maps and thus the same for each point in one set of variables. They are generally smaller than the intrinsic scatter in the correlations. Therefore we calculated in the log-log plane the ordinary least-squares bisector (Isobe et al. 1990) for the points in the two maps that are compared using the modified program code distributed by Feigelson. We note that with radio brightness on the Y-axis and FIR brightness on the X-axis the slope of the linear regression line of Y on X may be significantly smaller than the slope of the bisector if the correlation is not very good.

In order to judge the quality of the correlation, we also calculated the correlation coefficient c and the value of t (Student t-test) which indicates the probability that a correlation is accidental. For $t > 3$ and a number of points in the sample $N > 30$ this probability is < 0.003 implying that the correlation is highly significant at the 3σ level (Wall 1979). Values of t between 2.1 and 3.0 indicate a weak correlation. The value of t was calculated from the equation

$$t = c\sqrt{\frac{N-2}{1-c^2}}\ . \tag{2}$$

As the FIR properties of the bulge region ($R < 30'$) (Walterbos & Schwering 1987) differ from those of the outer disk ($30' < R < 90'$) we chose only pixels between 30 and 90 arcminutes distance from the centre and analyzed the inner region separately (see Sect. 4.4). The distances between two chosen pixels of $7'$ for maps at $5'$ resolution, $5'$ for maps at $3'$ resolution and $3\farcm5$ for maps at $2'$ resolution, ensure statistical independence of the points. Changing the position of the grid of pixels used for the correlations did not affect the results significantly, not even for the inner disk where the samples are fairly small. Only pixels with intensities above twice the r.m.s noise were taken into the samples.

Table 1 lists the radio continuum and FIR maps used for the correlations. The results of the complete sets of correlations are presented in Appendix B. A discussion of systematic errors is given in Appendix C.

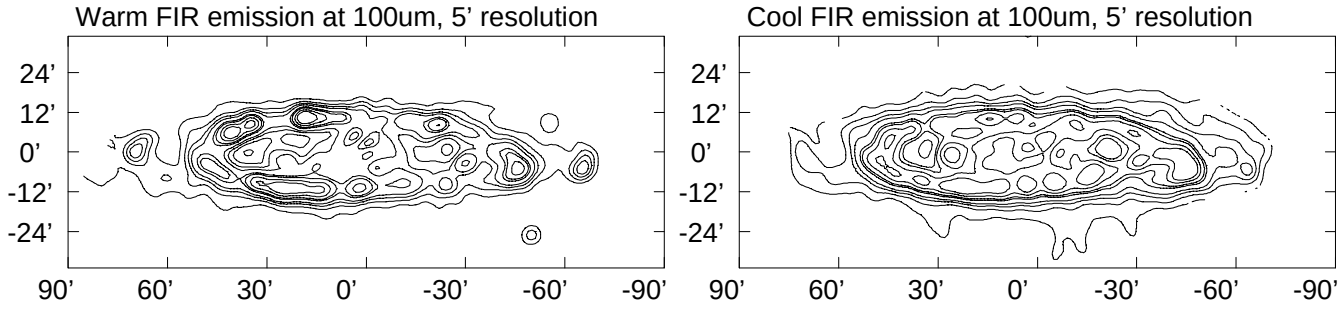

Fig. 4. Warm (27 K) and cool (19 K) dust emission at 100 μm from M 31 at $5'$ resolution derived from the 60 μm and 100 μm maps without nuclear point source. The contour lines in the maps indicate 2, 4, 6, 8, 12, 16 and 20 times the r.m.s. noise of the 100 μm FIR map.

Table 1. The radio continuum and FIR maps used for the correlations

		Resolution
	Radio continuum maps	
6 cm radio	The new Effelsberg survey at λ6.3 cm	$5'$, $3'$
11 cm radio	The Effelsberg map at λ11.1 cm	$5'$
20 cm radio	The combined Effelsberg-VLA map at λ20.5 cm	$5'$, $3'$, $2'$
Thermal (20 cm)	Thermal radio calculated with fixed nth. spectral index	$5'$
Nonthermal (20 cm)	Nonthermal radio calculated with fixed nth. spectral index	$5'$
	FIR maps	
Cool dust	The colour-colour decomposed cool FIR map	$5'$, $3'$, $2'$
Total FIR	The sum of $2.58 * 60\,\mu\mathrm{m} + 100\,\mu\mathrm{m}$ flux (see e.g. Helou et al. 1988)	$5'$, $3'$, $2'$
Warm dust	The colour-colour decomposed warm FIR map	$5'$, $3'$, $2'$

4.2. Correlations between total radio and total FIR emission for $30' < R < 90'$

At $5'$ resolution we first correlated the total radio and total FIR maps. Between 11 cm radio and total FIR we found a tight correlation with a slope of 0.80 ± 0.04, a correlation coefficient c of 0.90 ± 0.02 and $t = 18.3$ (Fig. 5a, Table B1). The quality of this correlation is almost as good as published global correlations between the integrated flux densities of galaxies. Of course the correlations within one galaxy have a smaller dynamic range, but the points are still spanning about 2 orders of magnitude.

An argument often used against the physical significance of correlations within a galaxy is that the emission of all components of the interstellar medium decreases with radius. It is clear that this will introduce an additional effect that may change the slope and tightness of correlations or even create apparent correlations. In order to be able to analyze the purely local relationship between radio continuum and FIR radiation, we corrected the maps for the radial dependencies. The intensity was averaged in rings around the centre of 2 kpc width in the plane of M 31, and a linearly interpolated curve was drawn through the means. Each point in the map was then divided by the value of the interpolated function at the appropriate radius. As the resulting maps show no radial decrease anymore, correlations between them should be free of radial effects. A comparison of an uncorrected and a corrected correlation plot is shown in Fig. 5.

After application of the radial correction significant correlations between radio continuum and FIR maps were still found. For example, between 11 cm radio and the total FIR map the slope of the correlation is 0.88 ± 0.07, with $t = 7.98$ and a correlation coefficient c of 0.67 ± 0.06 (Table B2, Fig. 5b). Although these values indicate a weaker correlation than without the radial correction (larger errors due to the smaller dynamic range), the correlation is still highly significant. The slopes of the correlations between total radio and total FIR in Tables B1 and B2 are smaller than those found for the global correlation between galaxies, which are larger than 1 (Niklas 1997).

In order to analyze possible effects of the beamsize on the radio-FIR correlations we computed a comparable set of correlations at the higher resolutions of $3'$ (corresponding to 600 pc $\times$ 2.8 kpc in M 31) and $2'$ (400 pc $\times$ 1.9 kpc), also after correction for the radial decrease of the radio and FIR intensities.

At $3'$ resolution the λ11 cm map is not available, so we computed the correlation between the λ20 cm radio map and total FIR. The slope is 1.00 ± 0.05, $t = 5.23$ and $c = 0.39 \pm 0.07$ (N=153 pixels) (Table 3).

At $2'$ resolution the slope between λ20 cm radio and total FIR is 0.76 ± 0.04, $t = 9.40$ and $c = 0.48 \pm 0.05$ (N=290 pixels) (Table 4).

Also the correlations at $3'$ and $2'$ resolution are highly significant.

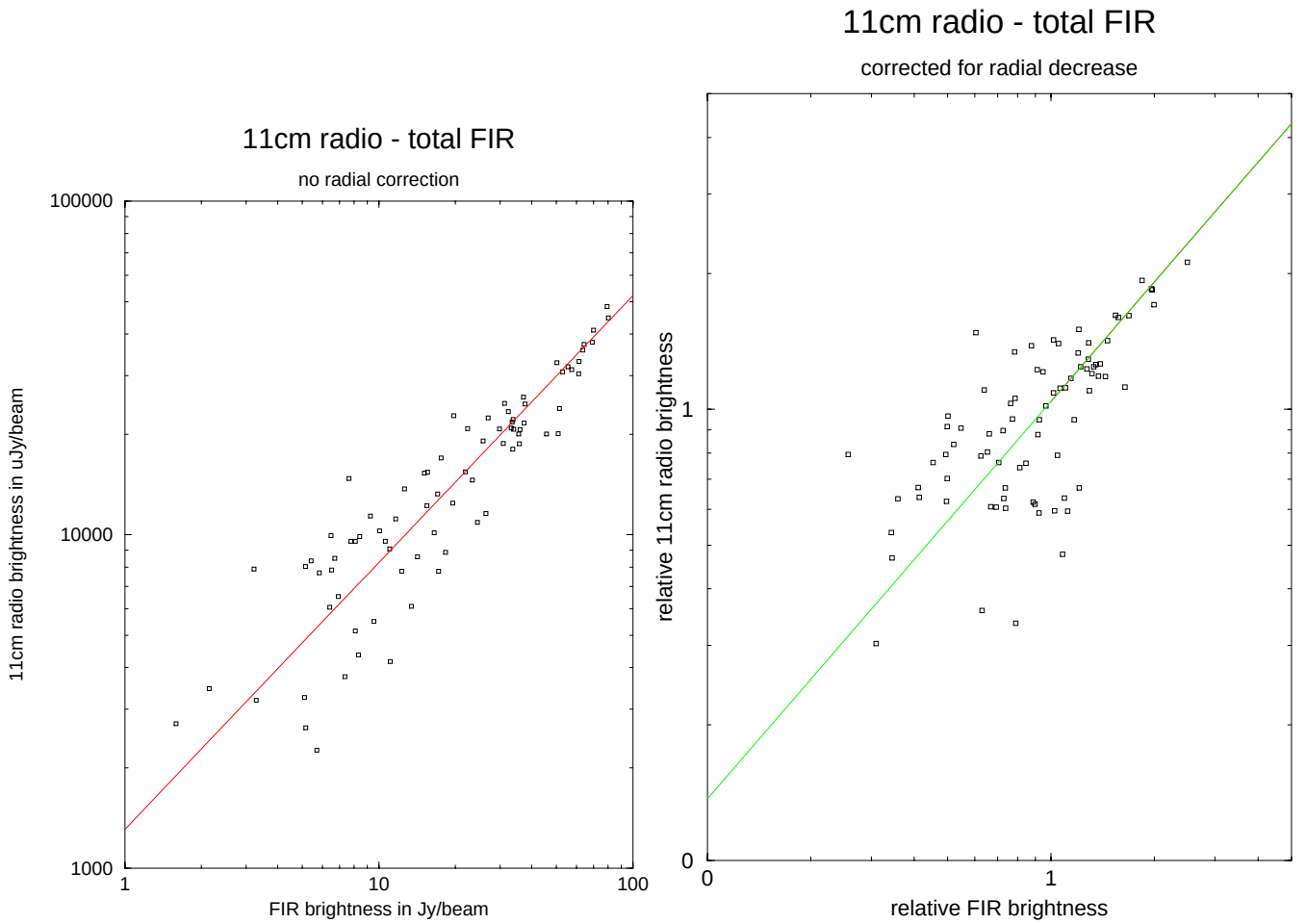

Fig. 5. Two examples of correlation plots for $30' < R < 90'$: a. 11 cm radio-total FIR (left) and b. the same correlation after application of the radial correction to both maps (right). Both correlations were derived from $5'$ resolution maps. The slopes of the bisectors are 0.80±0.04 and 0.88±0.07, respectively.

Table 2. Radio-FIR correlations for $30' < R < 90'$ at $5'$ resolution, radially corrected

Y	X	bisector slope	N	c	t
20 cm total radio	total FIR	0.97±0.08	79	0.67±0.07	7.31
thermal radio (20 cm)	warm dust	1.17±0.13	43	0.70±0.08	6.32
thermal radio (20 cm)	cool dust	1.31±0.22	43	0.36±0.14	2.45
nonthermal radio (20 cm)	warm dust	0.71±0.09	79	0.25±0.11	2.28
nonthermal radio (20 cm)	cool dust	0.80±0.09	80	0.43±0.09	4.19

4.3. Correlations between radio and FIR components for $30' < R < 90'$

More information about the physical mechanisms is expected from the correlations between the various components of radio and FIR emission. The most important results of the correlations at **5′ resolution** are listed in Table 2. The full set of results is given in Table B2.

The thermal radio emission correlates very well with warm dust emission (see Fig. 6a). The correlation is nearly as good as the total-radio/total-FIR correlation. Although the correlation between nonthermal radio and cool dust (Fig. 6b) is not as good as the thermal-radio/warm-dust correlation, it is still very significant statistically ($t = 4.19$). The cross-correlations are almost insignificant ($2.1 < t < 3.0$). The slopes of the correlations involving the thermal radio emission are slightly steeper than unity and those involving the nonthermal emission are flatter than unity.

At the resolution of 3′ we could only use the total-intensity maps at λ20 cm and λ6 cm (see Sect. B.4). A comparison with the results at $5'$ gives information on the dependence of the correlations on linear scale. In Table 3 the correlations are listed. The slopes of the total-radio/total-FIR correlations agree with unity. The correlations with warm dust are better than with cool dust, especially for λ6 cm. This effect is also seen at $5'$ resolution

Table 3. Radio-FIR correlations for $30' < R < 90'$ at $3'$ resolution, radially corrected

Y	X	bisector slope	N	c	t
20 cm total radio	total FIR	1.00±0.05	153	0.39±0.07	5.23
20 cm total radio	cool dust	1.10±0.07	148	0.36±0.07	4.63
20 cm total radio	warm dust	0.70±0.05	147	0.41±0.07	5.43
6 cm total radio	total FIR	0.94±0.06	140	0.66±0.05	10.30
6 cm total radio	cool dust	1.15±0.09	136	0.52±0.06	7.07
6 cm total radio	warm dust	0.72±0.06	135	0.68±0.06	10.75

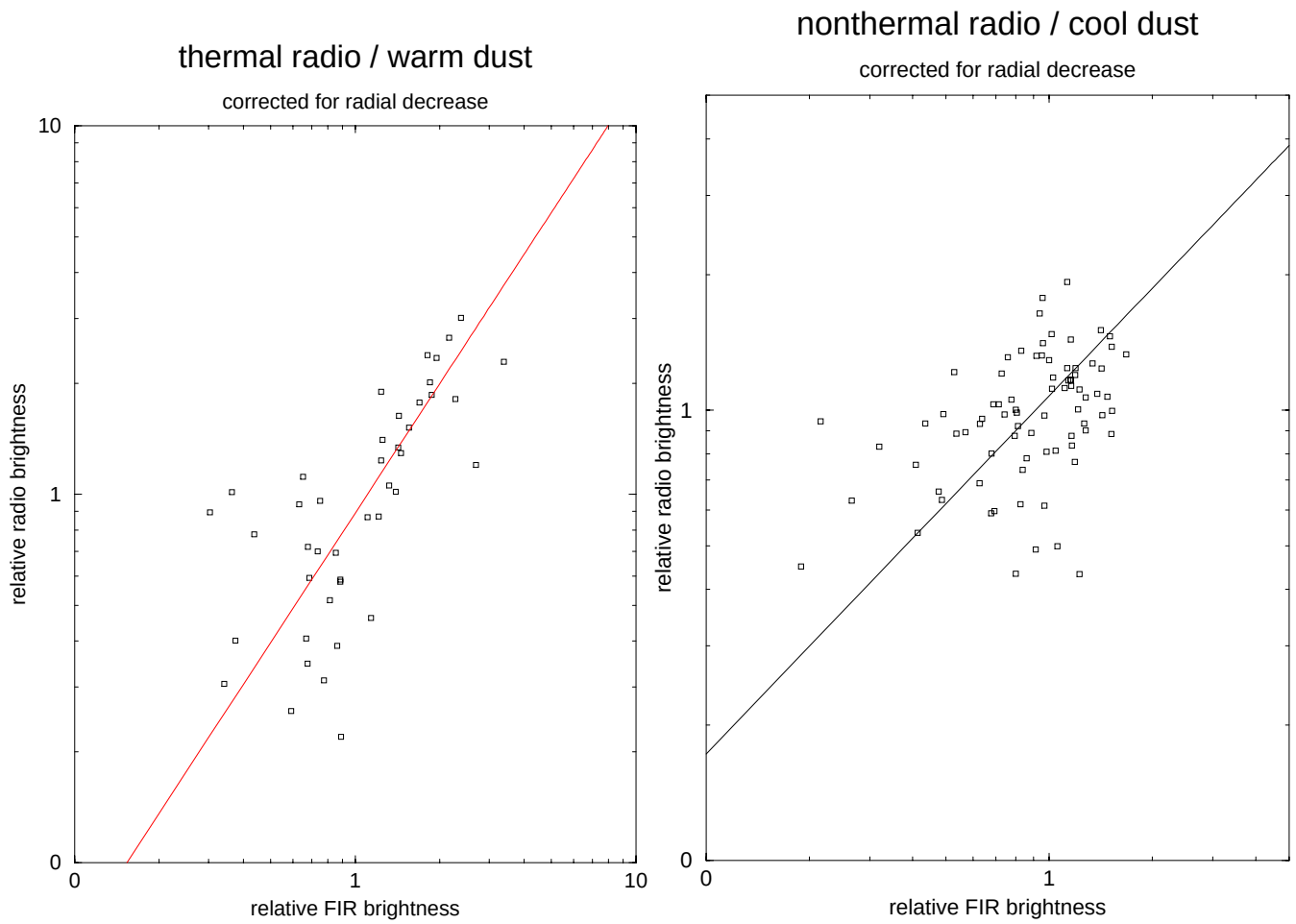

Fig. 6. Two examples of radially corrected correlation plots for $30' < R < 90'$: a. 20 cm thermal radio/warm dust (left) and b. 20 cm nonthermal radio/cool dust (right). The relative FIR brightness is on the X-axis, the relative radio continuum brightness on the Y-axis. Both correlations were derived from maps at $5'$ resolution. The slopes of the bisectors are 1.17 ± 0.13 and 0.80 ± 0.09.

(compare Table B2 in App. B) and is due to the correlation of thermal radio/warm dust which is much better than that of nonthermal radio/cool dust.

At **2′ resolution** only radio data at λ20 cm are available so we cannot separate the thermal and nonthermal components. The correlations of the total λ20 cm radio continuum map with the components of FIR emission are listed in Table 4. The correlations are very significant and the slopes are within three standard deviations from those at $5'$ and $3'$ resolution. As the slopes of the correlations obtained at $5'$ as well as at $3'$ ($2'$) resolution are not significantly different, we see no dependence of slope on linear scale in the range $1\,\mathrm{kpc} \times 5\,\mathrm{kpc}$ to $0.4\,\mathrm{kpc} \times 2\,\mathrm{kpc}$.

Table 4. Correlations between λ20 cm radio and FIR maps for $30' < R < 90'$ at $2'$ resolution, radially corrected

Y	X	slope	N	c	t
20 cm	total FIR	0.88±0.04	292	0.53±0.04	10.70
20 cm	cool dust	0.88±0.05	251	0.48±0.05	8.65
20 cm	warm dust	0.74±0.05	247	0.47±0.05	8.31

Table 5. Correlations between λ20 cm radio and total FIR maps at $3'$ and $2'$ in the inner disk ($R < 30'$) of M 31, radially corrected

Y	X	slope	N	c	t
$3'$ resolution					
20 cm	total FIR	1.11±0.18	24	0.55±0.15	3.11
$2'$ resolution					
20 cm	total FIR	1.04±0.11	49	0.49±0.11	3.85

4.4. Correlations in the inner disk of M 31

As there is little visible massive star formation going on in the inner disk ($R < 30'$), the physical mechanisms creating the FIR emission are expected to be different from those working in the outer regions of M 31. Does this lead to other correlation parameters than in the outer disk?

At $2'$ and $3'$ resolution there are enough independent pixels in the region inside $30'$ from the nucleus of M 31 to calculate correlations between total radio and FIR maps (see Table 5). The strong ISRF in the bulge region leads to a higher temperature of the diffuse dust than beyond $R \simeq 30'$ and would be assigned 'warm' by our decomposition routine. As the results of the FIR decomposition would be incomparable with those for the outer disk of M 31, we did not analyze the correlations with the cool and warm dust maps for the inner disk.

At $2'$ resolution 20 cm total radio and total FIR emission are significantly correlated. The weak correlation at $3'$ resolution agrees with that at $2'$ resolution within the errors. The slopes of the correlations between total radio and total FIR agree within errors with unity. Hence, they are consistent with the slopes of the total-radio/total-FIR correlations in the outer disk.

4.5. Summary of results

For the physical interpretation of the correlations we only consider the radially corrected ones which are free of large-scale effects:

- Within the M 31 disk ($30' < R < 90'$) there is a very significant correlation between total radio continuum and total FIR surface brightnesses on linear scales of about 1×5 kpc^2 (at $5'$ resolution) down to 0.4×2 kpc^2 (at $2'$ resolution). The correlation spans about one order of magnitude even after the correction for radial effects.
- In the area $30' < R < 90'$ on a scale of a few kpc ($5'$ resolution) there is a significant correlation between thermal radio and warm dust emission as well as between nonthermal radio and cool dust emission, but the latter correlation is not as tight as the former. At the same time, no significant correlations exist between thermal radio and cool dust emission and between nonthermal radio and warm dust emission.
- The slopes of the radio-FIR correlations within the disk of M 31 ($30' < R < 90'$) are generally smaller ($\lesssim 1$) than those of the corresponding correlations between the integrated flux densities of galaxies (> 1).
- In the inner region of M 31 ($R < 30'$) where there is little star formation, a significant correlation between total radio continuum at λ20 cm and total FIR emission exists on a linear scale of 0.4 ± 2 kpc^2 with the same slope ($\simeq 1$) as those in the outer disk.

5. Why are there radio-FIR correlations within M 31?

Our results (Sect. 4.5) for $30' < R < 90'$ at $5'$ resolution show that the significant local correlation between the total radio and total FIR emissions within the M 31 disk is due to the combination of a strong correlation between thermal radio and warm dust emission and a weaker correlation between nonthermal radio and cool dust emission. Could available models explain these correlations which hold on scales larger than a few kpc?

5.1. Existing models

At face value, these correlations are comparable to those found by Xu et al. (1994b) for the integrated radio and FIR fluxes of a sample of SAs and later-type galaxies. They interpreted the thermal-radio/warm-dust correlation as the result of massive ionizing stars powering both emissions, and the nonthermal-radio/cool-dust correlation as the effect of the common dependence of both emissions on intermediate mass stars ($5-20\,M_\odot$). Their non-ionizing UV radiation is largely responsible for the heating of the cool dust and at the end of their lives, as supernovae and supernova remnants, they accelerate the synchrotron emitting electrons.

For the thermal-radio/warm-dust correlation within the M 31 disk the interpretation of Xu et al. (1994b) is valid, as that correlation is a really local one in nature. On the other hand, Xu & Helou (1996b) showed that the cool diffuse dust in M 31 is *not* mainly heated by the non-ionizing UV radiation of intermediate stars: only 27% of the diffuse dust emission can be attributed to the heating by UV photons. The major part (73%) is due to heating by the optical radiation from solar-mass stars which are **not** supernova progenitors. Hence, the interpretation of Xu et al. (1994b) does not apply to the local nonthermal-radio/cool-dust correlation in M 31.

Since the cool-dust emission from M 31 is predominantly powered by low-mass stars, which implies that nearly 50% of the total FIR emission is coming from dust heated by the ISRF, models invoking the recent star-formation activity to link the radio and the FIR emission cannot explain the nonthermal-radio/cool-dust correlation in M 31. This seems to preclude almost all available models, including calorimeter theories, the model of Helou & Bicay (1993) and the model of Niklas & Beck (1997). Only when the recent star-forming activity were correlated with the formation of low-mass stars, a correlation between nonthermal radio and cool dust emission would be expected.

Recently, Ryder & Dopita (1994) found that the present-day star-formation rate (SFR) of a sample of 34 galaxies not only depends on the surface brightness of H I, but also on that of near infrared light, $\mathrm{SFR} \propto \sigma_{\mathrm{I}}^{0.64\pm0.37}$. As the surface brightness in near infrared is representative for the number of sub-solar mass

stars, there is a weak relationship between the numbers of young ionizing stars and stars of masses less than $1\,M_\odot$. We investigated this possibility for the outer disk of M 31 at a resolution of $5'$ by correlating the thermal radio emision which is due to massive ionizing stars and the surface brightness of blue light (Walterbos & Kennicutt 1988) which is mainly produced by stars of about $1\,M_\odot$. After radial correction of both emissions, a weak correlation exists between thermal radio and blue light which takes the form $\mathrm{SFR} \propto \sigma_\mathrm{B}^{1.8\pm0.3}$ with $c = 0.32$ and $t = 2.2$. Thus also within M 31 the number of ionizing stars ($M > 20\,M_\odot$) and of solar-mass stars are not entirely independent and could weakly link the thermal radio emission, part of the nonthermal emission and the warm dust emission to the cool dust emission heated by the ISRF. This may explain the weak correlation between thermal radio and cool dust emission (Table 2). On the other hand, we did not find a correlation between nonthermal radio and blue light, suggesting that the energy sources mainly powering these emissions are indeed uncorrelated in the outer disk of M 31. Therefore, the weak correlation between the number of massive ionizing stars and solar-mass stars cannot explain the significant correlation between nonthermal radio and cool dust emission observed within M 31.

5.2. The magnetic field-gas coupling model

The problem presented here is that nonthermal radio and cool dust emission, powered by different populations of stars, are surprisingly correlated with each other locally, although the correlation is not very tight (Fig. 5b). We showed in Sect. 5.1 that the correlation cannot be explained by a coupling of the energy sources. As the nonthermal emission is not correlated with the ISRF (as represented by the blue light), but is correlated with the emission from the cool dust, it must be correlated with the dust distribution. Therefore, the correlation could be essentially due to the coupling of the magnetic field to the neutral gas mixed with the cool dust. Berkhuijsen et al. (1993) and Berkhuijsen (1997) already presented evidence for such a coupling in the disk of M 31.

The surface brightness of M 31 at radio and other wavelengths is very low (about 1/4 of that of the Milky Way). Gräve et al. (1981) could not detect a radio halo around M 31, and Berkhuijsen et al. (1991) concluded that any emission from a thick radio disk must be two orders of magnitude weaker than that from the thick disk of the Milky Way (Beuermann et al. 1985). Berkhuijsen et al. (1991) also estimated that at λ92 cm the full thickness at half intensity of the nonthermal emission from the bright 'ring' in the SW, where the spiral arms are best separated, is less than 1.4 kpc. This corresponds to a thickness of less than 1 kpc at λ20 cm which is typical for normal spiral galaxies (Hummel 1990; Beck 1997). Furthermore, Braun (1991) derived a full thickness at half intensity of the H I of about 700 pc at the radial distance of the 'ring', indicating that M 31 does not have a thick gas disk. Hence, the disk could be 'optically thick' to cosmic-ray electrons although the nonthermal spectral index of -0.88 (Beck and Gräve 1982) is not as small as would be expected ($\alpha_\mathrm{n} \leq -1$) if radiative losses are important (Niklas & Beck 1997). In any case, the intensity of the nonthermal emission is $I_\mathrm{n} \propto n_0 B_\perp^{1-\alpha} l_\mathrm{n} \nu^{\alpha_\mathrm{n}}$, where n_0 is the volume density of the CR electrons per energy interval, $B_\perp$ the magnetic field strength perpendicular to the line of sight, l_n the pathlength through the emitting disk, ν the frequency of observation and α_n the nonthermal spectral index. How does I_n relate to the dust emission?

Compared to other spiral galaxies M 31 has an exceptionally low optical depth and even in UV it is optically thin (the face-on $\tau < 1$, Buat & Xu 1996). Therefore, unlike in most other galaxies which are optically thick in UV, the surface brightness of the cool (diffuse) dust emission from the M 31 disk, I_cool, is approximately proportional to the dust column density N_dust. More precisely, $I_\mathrm{cool} \propto I_0 \tau \propto I_0 N_\mathrm{dust}$, where I_0 is the intensity of the interstellar radiation field and τ the wavelength-averaged optical depth along the line of sight.

Thus the observed correlation between I_n and I_cool that we have to explain, takes the form

$$n_0 B_\perp^{1-\alpha_\mathrm{n}} l_\mathrm{n} \propto (I_0 N_\mathrm{dust})^\kappa \qquad (3)$$

at a given frequency, where κ is the observed exponent.

Since there is no observational evidence that I_0 (ISRF intensity) correlates locally with n_0 (CR electron density), the local nonthermal-radio/cool-dust correlation in M 31 must be due to the correlation between $l_\mathrm{n} B^{1-\alpha_\mathrm{n}}$ and N_dust. Available observations indicate that such a correlation is very plausible.
– Strong correlations between dust column density and gas column density were found in the Milky Way (Savage & Mathis 1979, and references therein) as well as in the M 31 disk (Xu & Helou 1996b). After correction for the radial gradient of the dust-to-gas ratio in M 31 Xu & Helou (1996b) obtained $N_\mathrm{dust} \propto N_\mathrm{H\,I}^\gamma$ where $\gamma = 1.01 \pm 0.02$. In Sect. 6.1 we argue that a very similar value of γ is expected if molecular gas were included. Assuming that, like in the Milky Way, the scale heights of the dust and the gas are the same, we can write $\rho_\mathrm{dust} \propto \rho_\mathrm{gas}^\gamma$, where ρ indicates volume density.
– Significant correlations between magnetic field strength $B_\perp$ and the volume density of the total gas ($\mathrm{H\,I} + 2\mathrm{H_2}$) were found both within the Milky Way (Fiebig & Güsten 1989; Berkhuijsen 1997) and in the M 31 disk (Berkhuijsen et al. 1993; Berkhuijsen 1997). The correlation is of the form $B \propto \rho_\mathrm{gas}^\beta$ where $\beta = 0.5 \pm 0.1$. Furthermore, Niklas & Beck (1997) found a good correlation between globally determined magnetic field strength and gas volume density for a sample of Shapley-Ames galaxies.

A test for the magnetic field-gas coupling model is to see whether it can explain the slope of the observed nonthermal-radio/cool-dust relation.

First we assume that the local scale heights of the synchrotron emitting disk and of the dust disk are proportional to each other. As the magnetic field is coupled to the gas this is a plausible assumption. The observed correlation then reduces to $n_0\, B_\perp^{1-\alpha_\mathrm{n}} \propto (I_0\, \rho_\mathrm{dust})^\kappa$.

Then we assume that I_0 and n_0 are constants in our problem. These assumptions are based on the following arguments:

a. The overall distribution of the optical radiation in M 31 is rather smooth (Walterbos & Kennicutt 1988). The variation is

mainly due to a radial gradient which should have been removed by the correction of the FIR maps.

b. While it is almost impossible to determine the intrinsic distribution of the CR electrons, the much smoother morphology of the nonthermal map compared to the thermal map suggests that they are also smoothly distributed in azimuth, possibly because they can diffuse rather freely along the regular field lines in the disk over several kpc. The radial correction may have also taken away most of the variation in the CR electron distribution with radius.

Nevertheless, 'constant' is always a relative definition in reality. If the variations of I_0 and n_0 are not much larger than those of $N_{\rm dust}$ and $l_{\rm n}B^{1-\alpha_{\rm n}}$, they may only contribute to the scatter in the correlation (which is indeed significant as shown in Fig. 5b) without destroying it.

Finally, with the above assumptions the expected slope of the nonthermal-radio/cool-dust correlation can be obtained from $I_{\rm n} \propto B_{\perp}^{1-\alpha_{\rm n}} \propto \rho_{\rm gas}^{\beta(1-\alpha_{\rm n})} \propto \rho_{\rm dust}^{\beta(1-\alpha_{\rm n})/\gamma} \propto I_{\rm cool}^{\beta(1-\alpha_{\rm n})/\gamma}$. Using the observed values of $\alpha_{\rm n} = -0.88 \pm 0.05$ (Beck & Gräve 1982), $\beta = 0.5 \pm 0.1$ (Berkhuijsen 1997) and $\gamma = 1.01 \pm 0.02$ (Xu & Helou 1996b) we expect a slope of $\kappa = 0.93 \pm 0.19$ which is within one standard deviation of the observed slope of 0.80 ± 0.09 at $5'$ resolution.

Thus our result shows that for galaxies optically thin to UV photons, like M 31, the coupling between magnetic field and gas indeed leads to a local nonthermal-radio/cool-dust correlation, even when the star-formation rate is very low. As in M 31 nonthermal radio emission and cool dust emission are the dominant components of the radio and FIR emission, respectively, their correlation contributes significantly to the total-radio/total-FIR correlation.

6. Discussion

In this section we concern ourselves with some aspects of the nonthermal-radio/cool-dust correlation in M 31.

6.1. Equipartition between CR particles and magnetic fields?

In order to explain the slope of the observed nonthermal-radio/cool-dust correlation with our magnetic field-gas coupling model, we assumed that the volume density of the relativistic electrons n_0 is approximately constant at a given radius which leads to the relation $I_{\rm n} \propto B^{1-\alpha_{\rm n}}$ for the nonthermal intensity. This implies that there is *no* equipartition between the energy densities of the CR particles (assumed to be proportional to the energy density of the CR electrons) and magnetic fields. In the case of equipartition $n_0 \propto B^2$ and $I_{\rm n} \propto B^{3-\alpha_{\rm n}}$ (Pacholczyk 1970) leading to $\kappa = 1.94$, much larger than the observed slope of 0.80 ± 0.09. This discrepancy seems to indicate that equipartition does not hold on a scale of a few kpc. As this would be an important conclusion, we first investigate whether in the case of equipartition a change in one of our other assumptions could explain the observed slope.

The observed relationships between magnetic field strength and gas density for M 31, the Milky Way and a Shapley-Ames sample of galaxies (Berkhuijsen et al. 1993; Berkhuijsen 1997; Niklas & Beck 1997) are based on the assumption of energy equipartition between CR particles and magnetic fields. They suggest $\beta = 0.5 \pm 0.1$ on kpc as well as on global scales. However, the values of β were obtained from data not corrected for the general radial decrease of the emission. Also the conversion factor $X_{\rm CO} = I_{\rm CO}/N_{\rm H2}$ is not well known. Thus we must await improved determinations of β to see whether it could be a factor of 2 lower to yield a correlation slope $\kappa < 1$ in case of equipartition. On the other hand, measurements of the magnetic field strength in dense clouds in the Milky Way via the Zeeman effect (Fiebig & Güsten 1989), where the assumption of equipartition does not enter the calculation of B, also indicate $\beta = 0.5 \pm 0.1$ on small scales of up to 100 pc. This is indeed expected for a field "frozen" into the gas (e.g. Zeldovich et al. 1983; Fleck 1983). Thus our adopted value of $\beta = 0.5 \pm 0.1$ seems quite plausible even if equipartition is not valid on kpc scales.

If equipartition were valid, the slope of the nonthermal-radio/cool-dust correlation could be < 1 if the value of γ in $N_{\rm dust} \propto N_{\rm gas}^{\gamma}$ were ≥ 2. Xu & Helou (1996b) obtained $\gamma = 1.01 \pm 0.02$ for the correlation between dust and H I, whereas we really need to know the slope of the correlation between dust and total gas (H I + $2H_2$). But as their correlation refers to regions of diffuse dust, in which little molecular gas is expected, inclusion of H_2 should have a minor effect on the value of γ. Furthermore, Bohlin et al. (1978) found a linear relationship both for $E_{\rm B-V} - N_{\rm HI}$ and for $E_{\rm B-V} - N_{\rm gas}$ in the solar neighbourhood. Thus γ is likely to be close to unity.

As it seems unlikely that in the case of equipartition the slope of the observed nonthermal-radio/cool-dust correlation can be explained by a change in our adopted values of β and γ, we are forced to conclude that on the scale of our observations at $5'$ resolution, a few kpc, equipartition in M 31 does not hold. Interestingly, Bertsch et al. (1993), using the observed distributions of γ-rays and neutral gas in the Milky Way, derived a scale length of 2 kpc for the coupling between CR particles and total gas. As the magnetic field is coupled to the gas on all scales, this also suggests that equipartition does not hold on scales smaller than a few kpc. Scales of up to a few kpc are typical for star-forming regions containing gas complexes, ionizing stars, supernovae and supernova remnants. It seems quite plausible that in such turbulent regions equipartition is not valid, whereas on larger scales equipartition holds.

Interestingly, Urbanik et al. (1994) also suggested that energy equipartition between cosmic rays and magnetic fields may not hold locally in M 31. Their conclusion is based on models for the total radio emission calculated from the FIR emission at 100μm assuming that the FIR emission traces the star-formation rate in M 31. As this assumption is not correct, it is not clear whether they would come to the same conclusion starting from more realistic assumptions for M 31.

We note that in Fig. 6b the relative nonthermal emission after the radial correction varies only about a factor of 2 around the mean correlation. Without equipartition this implies azimuthal variations in magnetic field strength of $2^{1/1.88} = 1.4$, corresponding to variations of about a factor 2 in the density of the

gas to which the field is coupled. As such variations seem quite normal within a galaxy there does not seem to be an observational argument against a decoupling of CR density and magnetic fields on kpc scales.

6.2. The correlation slopes: non-linearity?

A problem often discussed is the non-linearity of the correlation. Whereas in the past the non-unity slope of global correlations was attributed to a dust component heated by radio-quiet stars of $5 - 20\,\mathrm{M}_\odot$ (Condon et al. 1991; Xu et al. 1994b), other authors claimed that the nonthermal-radio/FIR correlation is inherently nonlinear with a slope of about 1.3 (Chi & Wolfendale 1990; Price & Duric 1992; Niklas 1997). Niklas (1997) showed that the total-radio/total-FIR correlation flattens to a slope of 1.1 for low-brightness galaxies like M 31. This flattening may indicate the increasing importance of dust heated by the ISRF in galaxies of low brightness, in which case the coupling between magnetic field and gas becomes the dominating mechanism in the radio/FIR correlation.

The slope of the nonthermal-radio/cool-dust correlation at $5'$ resolution within M 31 is smaller than 1. However, since the mechanism of the local correlation in M 31 is likely to be different from that of the global correlation (Sect. 5.2), a direct comparison between their slopes may not be appropriate. On the other hand, even for galaxies in which the dust heating is dominated by massive stars (e.g. NGC 6946), the slope of the local total-radio/total-FIR correlation (without correction for radial effects) is also smaller than unity (Marshall & Helou 1995; Lu et al. 1996), significantly smaller than the slope of the global correlation for such galaxies. This mainly reflects the difference in radial scale length which is larger for the radio than for the FIR emission due to the diffusion of CR electrons away from their sources (Bicay & Helou 1990; Marshall & Helou 1995; Lu et al. 1996). This shows that the radial correction is important; after this correction the correlation slopes within these galaxies may increase as we found for M 31.

6.3. Other models

Above, we argued that none of the models available in the literature can explain the nonthermal-radio/cool-dust correlation because they all assume that the correlation is due to the common dependence of the two emissions on the recent star-formation activity, whereas the cool dust in M 31 is mainly heated by the radiation of old stars. However, the magnetic field-gas coupling model proposed in Sect. 5.2 bears some similarities with other models for optically thin galaxies. Therefore we discuss the models of Helou & Bicay (1993) and Niklas & Beck (1997) below.

6.3.1. Model of Helou and Bicay

In addition to the coupling between the energy sources of the two emissions (L_{CR} and L_{heat}), Helou & Bicay (1993) assumed that the escape rates of the CR electrons and the dust-heating photons are coupled as the result of coupling between the magnetic field and the dust. This latter relation is exactly what our model is based on, but the assumption of the common dependence of the radiation energy sources on the recent star formation is not valid for M 31. Furthermore, their model predicts that the nonthermal-radio/cool-dust correlation flattens to a slope of unity for luminous galaxies, whereas Niklas (1997) showed that the slope is about 1.1 for low-brightness galaxies and steepens to 1.5 for bright galaxies. Another point is that the model of Helou and Bicay implies a correlation between the nonthermal spectral index and the magnetic field strength, but Niklas & Beck (1997) did not find a correlation between these quantities.

6.3.2. Model of Niklas and Beck

Niklas & Beck (1997) assumed that the FIR emission is coupled to the star-formation rate which in turn is determined by the gas density. As discussed above, this assumption is not applicable to the cool-dust emission in M 31 which is confirmed by the lack of a significant correlation between thermal-radio and cool-dust emission (see Table 2).

Furthermore, several of the assumptions of Niklas & Beck may hold on global scales but not on local scales of a few kpc. For example, their model predicts that the thermal emission is nearly linearly proportional to the nonthermal emission. However, our data at $5'$ do not show such a correlation. The correlation is probably destroyed by the diffusion of the CR electrons away from their sources, which is especially efficient in the regular magnetic field of M 31. Also our decomposition method may work against the detection of local correlations between thermal and nonthermal emission. We assumed a constant nonthermal spectral index of -0.88, whereas near supernova remnants it should be close to -0.5. This emission is partly assigned to the thermal component by our algorithm. Hence, near star-forming regions the thermal emission is overestimated and the nonthermal emission is underestimated.

Niklas & Beck also assumed energy equipartition between CR particles and magnetic fields. This assumption may break down on scales of a few kpc (see Sect. 6.1).

6.3.3. Compilation of models

In Table 6 we list the presently existing models for the observed radio/FIR correlations of galaxies and the basic assumptions of these models.

Early models assume that massive ionizing stars are the only energy sources of the dust heating and the radio emission, whereas our model assumes this only to explain the thermal-radio/warm-dust correlation. We propose that the nonthermal-radio/cool-dust correlation arises from dust heated by the ISRF mixed with the neutral gas, to which the magnetic field is coupled that is responsible for the nonthermal emission.

We note that if $I_{\mathrm{n}} \propto I_{\mathrm{cool}}^{\kappa}$ with $\kappa = \beta(1-\alpha_{\mathrm{n}})/\gamma$, we expect $\kappa > 1$ for the nonthermal/cool-dust correlation in galaxies with a steep spectral index $\alpha_{\mathrm{n}} < -1$.

Table 6. Models to explain radio/FIR correlations

Model	Basic assumptions	Optical thickness UV	CR	Expected slope	Global/Local
Calorimeter Völk (1989)	a. Massive stars power radio and FIR emission	thick	thick	1	global
Helou & Bicay (1994)	a. as above b. Proportional creation rates of UV photons and CR particles c. $B \propto \rho_{\rm gas}^{0.5}$	thin	thin	1	global
Niklas & Beck (1997)	a. as above c. $B \propto \rho_{\rm gas}^{0.5}$ d. $n_{\rm CR} \propto B^2$ e. $SFR \propto \rho_{\rm gas}^{1.4}$	thick	thin	> 1	global + local
This paper	For thermal/warm-dust correlation a. as above	–	–	1	global + local
	For nonthermal/cool-dust correlation c. $B \propto \rho_{\rm gas}^{0.5}$ determines nonthermal emission f. ISRF heats cool dust	thin	irrelevant	$\{ \leq 1$ for $\alpha_{\rm n} \geq -1.0$ $\{ > 1$ for $\alpha_{\rm n} < -1.0$	global + local

7. Conclusions

We have made a thorough comparison between a set of radio maps (including the new λ6 cm and the high-resolution map at λ20 cm) and FIR maps obtained from high-resolution IRAS observations of M 31. At the resolutions of $5'$, $3'$ and $2'$ the total surface brightnesses of the two emissions are significantly correlated, even after correction for the general radial decrease (Fig. 5, Tables 2, 3 and 5). The slopes of the radially corrected correlations are all consistent with unity.

For the region $30' < R < 90'$ at $5'$ resolution the data enabled a decomposition of the radio maps into maps of thermal and nonthermal (synchrotron) emission (Fig. 3), and of the FIR maps into maps of warm ($T_{\rm d} = 27$ K) and cool ($T_{\rm d} = 19$ K) dust emission (Fig. 4). Thermal radio emission correlates significantly with warm dust emission and nonthermal radio with cool dust emission (Fig. 6, Table 2). Correlations between other combinations of radio and FIR components are insignificant.

The correlation between thermal radio and warm dust can be explained by the common dependence of these emissions on massive ionizing stars. It also has a slope close to unity.

The correlation between nonthermal radio and cool dust has a slope of 0.80 ± 0.09 and is physically more interesting. As the cool dust emission from M 31 is predominantly powered by the optical radiation from relatively old stars, all available models for the radio/FIR correlation which universally assume that the basic reason for the correlation is the common dependence of the two emissions on the recent star formation, are deemed irrelevant. In Sect. 5.2 we propose a new model to explain the nonthermal-radio/cool-dust correlation based on a coupling of the magnetic field to the gas mixed with the dust (magnetic field-gas coupling and gas-dust coupling). This yields satisfactory agreement with the observed slope if energy equipartition between cosmic-ray particles and magnetic fields does not hold on scales of a few kpc.

Our results suggest that for galaxies optically thin to UV photons, like M 31, magnetic field-gas coupling indeed leads to a nonthermal-radio/FIR correlation even when the recent star-formation rate is very low. However, further studies should clarify why optically thick galaxies, in which radio and FIR emission depend on the same energy sources, and optically thin galaxies with little star formation like M 31 follow approximately the same radio/FIR relation.

Acknowledgements. We thank Dr. R. Beck for interesting discussions, valuable suggestions and useful comments on the manuscript. We are grateful to Dr. N. Devereux for putting the Hα map at our disposal in digital form.

Appendices A, B and C can be found in the electronic version of this paper.

References

Aumann H.H., Fowler J.W., Melnyk M., 1990, AJ 99, 1674
Baade W., 1958, Ric. Astron. Specola. Astron. Vatic. 5, 1
Beck R., 1997. In: Lesch H., Dettmar R.-J., Mebold U., Schlickeiser R. (eds) Proc. 156. WE-Heraeus-Seminar, The Physics of Galactic Halos. Akademie Verlag, Berlin, p. 135
Beck R., Golla G., 1988, A&A 191, L9
Beck R., Gräve R., 1982, A&A 105, 192
Beck R., Berkhuijsen E.M., Wielebinski R., 1980, Nat 283, 272
Beck R., Berkhuijsen E.M., Hoernes P., 1998, A&A (in press)
Berkhuijsen E.M., 1977, A&A 57, 9
Berkhuijsen E.M., 1997. In: Lesch H., Dettmar R.-J., Mebold U., Schlickeiser R. (eds.) Proc. 156. WE-Heraeus-Seminar, The Physics of Galactic Halos. Akademie Verlag, Berlin, p. 155
Berkhuijsen E.M., Wielebinski R., Beck R., 1983, A&A 117, 141

Berkhuijsen E.M., Golla G., Beck R., 1991. In: Bloemen H. (ed.) Proc. IAU Symp. 144, The Interstellar Disk-Halo Connection in Galaxies. Kluwer, Dordrecht, p. 233
Berkhuijsen E.M., Bajaja E., Beck R., 1993, A&A 279, 359
Bertsch D.L., Dame T.M., Fichtel C.E. et al., 1993, ApJ 416, 587
Beuermann K., Kanbach G., Berkhuijsen E.M., 1985, A&A 17, 153
Bicay M.D., Helou G., 1990, ApJ 362, 59
Boggs P.T., Byrd R.H., Rogers J.E., Schnabel R.B., 1992, ODRPACK User's Reference Guide. U.S. Department of Commerce, National Institute of Standards and Technology, Gaithersburg, MD 20899, June 1992
Bohlin R.C., Savage B.D., Drake J.F., 1978, ApJ 224, 132
Boulanger F., Pérault M., 1988, ApJ 330, 964
Braun R., 1991, ApJ 372, 54
Buat V., Deharveng J.M., 1988, A&A 195, 60
Buat V., Xu C., 1996, A&A 306, 61
Chi X., Wolfendale A.W., 1990, MNRAS 245, 101
Ciardullo R., Rubin V.C., Jacoby G.H., Ford H.C., Ford W.K. Jr., 1988, AJ 95, 438
Condon J.J., 1992, ARA&A 30, 575
Condon J.J., Anderson M.L., Helou G., 1991, ApJ 376, 95
de Jong T., Klein U., Wielebinski R., Wunderlich E., 1985, A&A 147, L6
Devereux N.A., Price R., Wells L.A., Duric N., 1994, AJ 108, 1664
Emerson D.T., 1974, MNRAS 169, 607
Fiebig D., Güsten R., 1989, A&A 214, 333
Fitt A.J., Howarth N.A., Alexander P., Lasenby A.N., 1992, MNRAS 255, 255
Fleck Jr. R.C., 1983, ApJ 264, 139
Gioia I.M., Gregorini L., Klein U., 1982, A&A 116, 164
Gräve R., Emerson D.T., Wielebinski R., 1981, A&A 98, 260
Helou G., 1986, ApJ 311, L33
Helou G., M.D. Bicay M.D., 1993, ApJ 415, 93
Helou G., Soifer B.T., Rowan-Robinson M., 1985, ApJ 298, L7
Helou G., Khan I.R., Malek L., Boehmen L., 1988, ApJS 68, 141
Hummel E., 1990. In: Fabbiano G., Gallagher J.S., Renzini A. (eds.) Windows on Galaxies. Kluwer, Dordrecht, p. 141
Isobe T., Feigelson E.D., Akritas M.G., Babu G.J., 1990, ApJ 364, 104
Lisenfeld U., Völk H.J., Xu C., 1996, A&A 306, 677
Lu N.Y., Helou G., Tuffs R. et al., 1996, A&A 315, L153
Marshall K.A., Helou G., 1995, ApJ 445, 599
Niklas S., 1997, A&A 322, 29
Niklas S., Beck R., 1997, A&A 320, 54
Pacholczyk A.G., 1976, Radio Astrophysics. W.H. Freeman, San Francisco
Pellet A., Astier N., Viale A. et al., 1978, A&AS 31, 439
Pooley G.G., 1969, MNRAS 144, 101
Price R., Duric N., 1992, ApJ 401, 81
Puget J.L., Léger A., 1989, ARA&A 27, 161
Rice W., Lonsdale C.J., Soifer B.T. et al., 1988, ApJS 68, 91
Ryder S.R., Dopita M.A., 1994, ApJ 430, 142
Savage B.D., Mathis J.S., 1979, ARA&A 17, 73
Soifer B.T., Houck J.R., Neugebauer G., 1987, ARA&A 25, 187
Urbanik M., Otmianowska-Mazur K., Beck R., 1994, A&A 287, 410
Völk H.J., 1989, A&A 218, 67
Völk H.J., Xu C., 1994, Infrared Phys. Technol. 35, 527
Wall J.V., 1979, QJRAS 20, 138
Walterbos R.A.M., 1987. In: Pudritz R.E., Fich M. (eds.) Galactic and Extragalactic Star Formation. Kluwer, Dordrecht, p. 361
Walterbos R.A.M., Kennicutt Jr. R.C., 1988, A&A 198, 61
Walterbos R.A.M., Schwering P.B.W., 1987, A&A 180, 27
Wunderlich E., Klein U., Wielebinski R., 1987, A&AS 69, 487
Xu C., 1990, ApJ 365, L47
Xu C., Helou G., 1994, ApJ 426, 109
Xu C., Helou G., 1996a, ApJ 456, 152
Xu C., Helou G., 1996b, ApJ 456, 163
Xu C., Klein U., Meinert D., Wielebinski R., Haynes R.F., 1992, A&A 257, 47
Xu C., Lisenfeld U., Völk H.J., Wunderlich E., 1994a, A&A 282, 19
Xu C., Lisenfeld U., Völk H.J., 1994b, A&A 285, 19
Zeldovich Y.B., Ruzmaikin A.A., Sokoloff D.D., 1983, Magnetic Fields in Astrophysics. Gordon and Breach, New York